Journal of Power Sources 343 (2017) 1–10

Contents lists available at ScienceDirect

Journal of Power Sources

journal homepage: www.elsevier.com/locate/jpowsour

Co- and Ce/Co-coated ferritic stainless steel as interconnect material for Intermediate Temperature Solid Oxide Fuel Cells

Hannes Falk-Windisch*, Julien Claquesin, Mohammad Sattari, Jan-Erik Svensson, Jan Froitzheim

Chalmers University of Technology, Department of Chemistry and Chemical Engineering, Division of Energy and Materials, Kemivägen10, SE-41296, Gothenburg, Sweden

HIGHLIGHTS

- Co- and Ce/Co-coatings (~600 nm) are investigated for >3000 h at IT-SOFC temperatures.
- Cr species evaporation is effectively impeded for more than 3000 h.
- Low oxidation rates and ASR are observed.
- A beneficial effect of Ce is observed even at IT-SOFC relevant temperatures.

ARTICLE INFO

Article history:
Received 11 December 2016
Received in revised form
5 January 2017
Accepted 9 January 2017

Keywords:
Interconnect
Solid oxide fuel cell
Corrosion
Cr vaporization
Area specific resistance
Coating

ABSTRACT

Chromium species volatilization, oxide scale growth, and electrical scale resistance were studied at 650 and 750 °C for thin metallic Co- and Ce/Co-coated steels intended to be utilized as the interconnect material in Intermediate Temperature Solid Oxide Fuel Cells (IT-SOFC). Mass gain was recorded to follow oxidation kinetics, chromium evaporation was measured using the denuder technique and Area Specific Resistance (ASR) measurements were carried out on 500 h pre-exposed samples. The microstructure of thermally grown oxide scales was characterized using Scanning Electron Microscopy (SEM), Scanning Transmission Electron Microscopy (STEM), and Energy Dispersive X-Ray Analysis (EDX). The findings of this study show that a decrease in temperature not only leads to thinner oxide scales and less Cr vaporization but also to a significant change in the chemical composition of the oxide scale. Very low ASR values (below 10 mΩ cm^2) were measured for both Co- and Ce/Co-coated steel at 650 and 750 °C, indicating that the observed change in the chemical composition of the Co spinel does not have any noticeable influence on the ASR. Instead it is suggested that the Cr_2O_3 scale is expected to be the main contributor to the ASR, even at temperatures as low as 650 °C.
© 2017 The Author(s). Published by Elsevier B.V. This is an open access article under the CC BY license (http://creativecommons.org/licenses/by/4.0/).

1. Introduction

Solid Oxide Fuel Cell (SOFC) technology offers several advantages over traditional combustion technologies, such as high electrical efficiency, low emissions, scalability, and high fuel flexibility [1,2]. Although this technology has great potential, expensive component materials in combination with unacceptable degradation rates have limited the commercial success of this technology to date. To tackle these two problems the development of new electrode and electrolyte materials that enable operation at lower temperatures has been highly prioritized. In fact several companies are currently able to produce SOFC systems that operate in a temperature range between 600 and 700 °C, compared to the common 750-850 °C for planar SOFC. Using this temperature regime the degradation rates are expected to be significantly lower, and some of the component materials can be substituted with less expensive materials, such as the interconnect material. The interconnect is a key component that electrically connects several cells in series, forming what is known as a stack. Besides connecting cells electrically, the interconnect also separates the air on the cathode side of one cell from the fuel on the anode side of the neighbouring cell. Since the SOFC is heated to high temperatures it is crucial that the Coefficient of Thermal Expansion (CTE) for the interconnect

* Corresponding author.
E-mail address: hannes.windisch@chalmers.se (H. Falk-Windisch).

http://dx.doi.org/10.1016/j.jpowsour.2017.01.045
0378-7753/© 2017 The Author(s). Published by Elsevier B.V. This is an open access article under the CC BY license (http://creativecommons.org/licenses/by/4.0/).

material is close to the CTE of the ceramic parts in the stack [3]. Other requirements for the interconnect material are high electrical conductivity, stability in both low and high pO_2, and gas tightness [3]. Furthermore, the material should to be easy to shape and inexpensive to manufacture in large volumes. Because of all these requirements, ferritic stainless steels that rely on the formation of a protective Cr_2O_3 layer have become the most popular choice for interconnect materials for planar SOFCs operating in temperature regimes between 600 and 850 °C. However, volatile chromium (VI) species are formed on the chromium-rich interconnect surface at these temperatures [4–7]. These species are then transported from the interconnect surface to the cathode, where they are either deposited or react with the cathode material to cause rapid cell degradation [8–15]. To solve the problem of chromium species vaporization, most interconnect steels are coated with a material that can significantly reduce chromium volatilization. Today Cobalt-based (Co) and Manganese-based (Mn) spinel (MCO) coatings have become the most common type of coatings. Kurokawa et al. [16] and Trebbels et al. [17] have shown that MCO coatings can mitigate Cr vaporization in humid air at 800 °C. In both studies MCO powder was sprayed on the steel surface, followed by a heat treatment process to densify the deposited powder. Cr vaporization measurements by Kurokawa and Trebbels showed that the ability of the MCO coating to mitigate Cr vaporization was dependent on the density of the coating. To achieve a high coating density, and for the coating to adhere well to the steel substrate, the heat treatment temperatures are commonly significantly higher than the desired SOFC operating temperature. This may lead to the formation of a rather thick Cr_2O_3 scale, causing a high electrical resistance. To avoid the heat treatment step, techniques such as plasma spraying [18] or Physical Vapour Deposition (PVD) [19] can be used to deposit dense MCO coatings. Another alternative to the ceramic MCO coatings is to coat the steel with a metallic Co- or a Co/Mn-layer. These metals are rapidly oxidized in air at the desired operating temperature of the fuel cell, and are therefore converted into Co- and Co/Mn-spinel coatings in-situ [20–22]. Furthermore, the Co_3O_4 layer that is formed on the exclusively Co-coated material can be transformed into a $(Co,Mn)_3O_4$ top-layer, due to outward Mn diffusion from the steel [23,24]. The possibility to mitigate Cr vaporization by coating the steel with metallic Co-coatings has been proven in several studies [20,21,23,25–27]. Moreover, these layers do not need to be very thick. Froitzheim et al. [23] showed that Cr vaporization can be reduced significantly for at least 3000 h at 850 °C by coating the stainless steel Sanergy HT with only 640 nm Co. The thin Co-coating in that study was applied by PVD. However, other researchers have shown that metallic Co- and Co/Mn-coatings can also be applied using electroplating [22,24], sol-gel deposition [28], and Pulsed Laser Deposition (PLD) [27]. If each interconnect is coated in a separate step, electroplating and sol-gel deposition can be considered as more cost-efficient techniques compared to PVD. PVD can however be used in a continuous process so that large volumes of steel can be pre-coated in a roll-to-roll processes [29]. The pre-coated steel coil can then be pressed into thousands of interconnects. In two recent studies we were able to show that pre-coated steel can be pressed into interconnects, without increasing chromium vaporization, due to the potential for the coating to heal upon exposure [25,30]. Thin metallic Co coatings can therefore be considered as a cost-effective option for mitigating chromium vaporization.

Furthermore, to reduce the oxide scale growth rate on the material, and in particular the growth of the Cr_2O_3 layer, which is the main contributor to an increase in electrical resistance over time, an additional coating consisting of 10 nm Cerium (Ce) can be added to the metallic Co coating [21,26,31]. Earlier investigations at 850 °C have shown that the addition of such a layer not only slows the oxide scale growth rate, but also the electrical scale resistance over time is significantly lower with the additional Ce coating [32–34]. Moreover, Harthoj et al. [24] showed that improved oxidation resistance, and as a consequence lower electrical resistance, can also be achieved by co-depositing CeO_2 particles in the electrodeposited Co coating. The beneficial effect of Ce is attributed to the well-known reactive element effect (REE) [35]. The above mentioned studies on both Co- and Ce/Co-coated steels, as well as the absolute majority of all studies on ferritic stainless steels as the interconnect material in SOFC, have been carried out at 800 °C or above, which is significantly higher than the 600–700 °C temperature regime that some of the newer SOFC systems are designed to operate at. To be able to substitute today's expensive, specially designed interconnect materials with less expensive materials for the SOFC systems that are able to operate in the lower temperature regime between 600 and 700 °C, it is crucial to study the degradation mechanisms stated above, Cr vaporization and oxide scale growth, in this lower temperature regime. Therefore, the aim of this study was to investigate metallic Co- and Ce/Co-coated ferritic stainless steel at 650 and 750 °C with regard to Cr vaporization, oxide scale growth, and microstructural and chemical evolution, as well as the effect these factors have on the electrical resistance of the oxide scale.

2. Materials and methods

Metallic Co- and Ce/Co-coated materials were produced by coating 0.2 mm thick sheets of the ferritic stainless steel Sanergy HT (chemical composition shown in Table 1) with 640 nm Co and 10 nm Ce + 640 nm Co. The Co and Ce/Co coatings were prepared by Sandvik Materials Technology using a Physical Vapour Deposition (PVD) process. 15 × 15 mm^2 coupons were cut from a Co, Ce/Co, and uncoated steel sheet and cleaned in acetone and ethanol using an ultrasonic bath. Since the coupons were cut, the edges (corresponding to 2.6% of the total surface area) were not coated. All samples were exposed in an as-received state, i.e. no further treatments were carried out before exposure. All exposures were carried out in an air-3% H_2O environment using a flow rate of 6000 sml min^{-1}. 3% water vapour was achieved by bubbling dry air through a heated water bath connected to a condenser containing water at a temperature of 24.4 °C. Two types of exposures were carried out; isothermal and discontinuous exposures. A series of samples was isothermally exposed for 500 h and Cr vaporization was simultaneously measured (isothermal exposures). A second series of samples was exposed for 3300 h, and the samples were cooled regularly to follow the mass gain over time (discontinuous exposures). Cr vaporization was measured for the last 300–500 h on the samples exposed discontinuously. Cr vaporization measurements were carried out using the denuder technique. A more detailed description of the denuder technique and the experimental setup can be found elsewhere [36].

In the isothermal exposure experiments two identical samples were exposed for each type of material in order to record Cr vaporization. In contrast, for the discontinuous long-term exposure two uncoated, two Co-coated, and two Ce/Co-coated samples were exposed together in the very same exposure. For the last 300–500 h, however, the three different materials were divided and Cr vaporization measurements were carried out in the same manner as for the isothermal 500 h exposures.

Area Specific Resistance (ASR) measurements were carried out ex-situ on the samples isothermally exposed for 500 h at 650 and 750 °C, as well as on samples that were exposed isothermally for 500 h at 850 °C. Ex-situ measurements were chosen to avoid any effect of the platinum (Pt) electrode material, which has been observed by Grolig et al. [32]. A sputter mask of 1*1 cm^2 was placed

Table 1
Composition of the studied steel Sanergy HT in weight % as specified by the manufacturer for the batch used.

Material	Manufacturer	Fe	Cr	C	Mn	Si	Mo	W	Nb	RE
Sanergy HT Batch: 531816	Sandvik Materials Technology	Bal.	22.4	0.01	0.25	0.07	0.93	<0.01	0.41	Zr

on the 500 h pre-oxidized samples and a very thin layer of Pt was sputtered on top of the oxide scale. After the sputtering step, the sputtered area was painted with Pt paste (Metalor 6926). These samples were then dried for 10 min at 150 °C, followed by a Pt sintering step for 1 h at the same temperature as the earlier exposure temperature (650, 750, or 850 °C). A Probostat (NorECs, Norway) test cell placed in a tubular furnace was used to measure ASR. The DC resistance was measured using a Keithley 2400 source meter in four-point mode and the applied current during the measurement was set to 100 mA/cm^2. To check for semiconductive behaviour, the ASR was monitored as the samples were cooled down.

The microstructure and chemical composition of the oxide scales were analysed using an FEI Quanta 200 FEG Environmental Scanning Electron Microscope (ESEM) equipped with an Oxford Instruments X-Max^N Energy Dispersive X-ray spectroscopy (EDX) detector and INCAEnergy software. Cross sections were prepared by using a Leica TIC3X Broad Ion Beam (BIB). A low-speed saw with a diamond blade was used to cut a sample in half to enable BIB cross-sections from the centre of the sample and not from the edges. Furthermore, Focused Ion Beam (FIB) milling and lift-out techniques were utilized to prepare a thin cross-sectional specimen from the Co-coated material exposed for 3300 h at 650 °C. For this purpose an FEI Versa 3D Dual Beam Focused Ion Beam/Scanning Electron Microscope (FIB/SEM) was used. Two layers of Pt were deposited on the area of interest to protect the sample from ion beam damage during milling, firstly using an electron beam, followed by an ion-beam-induced deposition. This sample was subsequently characterized by Scanning Transmission Electron Microscopy (STEM) using an FEI Titan 80–300 TEM equipped with an INCA X-Sight Oxford Instruments EDX detector.

3. Results

3.1. Gravimetric analysis

Fig. 1a shows the mass gain values for both the isothermal (500 h) and the discontinuous (up to 3300 h) exposures at 650 °C for uncoated, Co-coated, and Ce/Co-coated Sanergy HT. For the uncoated material a small increase in mass (during the first 100 h) followed by an almost linear loss in mass with continued exposure time can be seen, which is in line with earlier published data on uncoated Sanergy HT [37].

This type of mass gain behaviour is commonly associated with paralinear oxidation, where the mass gain value is the sum of parabolic oxide scale growth and simultaneous linear mass loss due to vaporization of the oxide scale [38,39]. Initially oxide scale growth is fast resulting in positive mass gain values, however, as the oxide scale thickens, mass loss due to vaporization of $CrO_2(OH)_2$ dominates. Such behaviour was not observed for the samples coated with Co and Ce/Co, and instead all coated samples increased in mass with time. Within the first 24 h of exposure all coated samples showed a rapid gain in mass (0.22 mg/cm^2 for samples coated with Ce/Co, and 0.27 mg/cm^2 for the samples only coated with Co at 650 °C). The 640 nm thin metallic Co-coating oxidized rapidly and this gain in mass corresponds to 0.21 mg/cm^2. At 650 °C this difference in mass gain between the Co- and the Ce/Co-coated material was constant over the duration of the entire experiment, indicating that the extra Ce layer did not have any effect except for in the initial oxidation phase.

Fig. 1b shows the mass gain values at 750 °C. The main difference between the two exposure temperatures for the uncoated material is a greater initial mass gain, followed by a steeper loss in mass at 750 °C than at 650 °C. For the coated materials a clear increase in mass with time was seen at 750 °C. A clear improvement with the extra 10 nm Ce-coating can be seen when comparing the Ce/Co- and the Co-coated material. Within the first 24 h of exposure the difference in mass gain between the Co- and the Ce/Co-coated materials was similar to that seen at 650 °C. However, after 3300 h of exposure the mass gain for the Ce/Co-coated material was 0.19 mg/cm^2 lower than the mass gain for the Co-coated material. It can therefore be concluded that the additional 10 nm Ce layer had a beneficial effect on mass gain behaviour at 750 °C.

3.2. Cr vaporization measurements

Fig. 2a shows the rate of Cr vaporization as a function of exposure time for the uncoated, the Co-coated, and the Ce/Co-coated

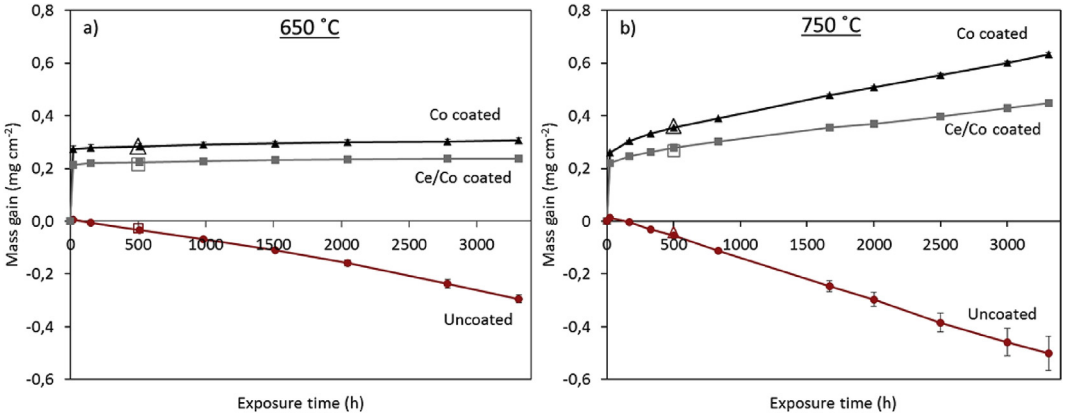

Fig. 1. Mass gain values at (a) 650 °C and (b) 750 °C for uncoated (red dots), Co-coated (black triangles), and Ce/Co-coated (grey squares) Sanergy HT exposed for up to 3300 h in air containing 3% H_2O with a flow rate of 6000 sml/min. Both isothermal (500 h) and discontinuous (3300 h) exposures are shown. The open markers at 500 h represent the mass gain from the isothermal exposures. The 500 h isothermal exposure values for the uncoated material are taken from a previous publication [37].

material exposed at 650 °C. The Cr vaporization rate for both the Co- and the Ce/Co-coated material was more than one order of magnitude lower than the Cr vaporization rate for the uncoated material and no clear difference in vaporization rate could be observed between the Co- and the Ce/Co-coated material. It is also interesting to note that the Cr vaporization rate did not change with time over 500–3300 h of exposure for the uncoated material or for the two coated materials.

Fig. 2b shows the Cr vaporization rates at 750 °C. Except for higher Cr vaporization rates for all materials as a consequence of the higher exposure temperature, the same trends seen in Fig. 2a at 650 °C are seen at 750 °C. Both the Co- and the Ce/Co-coatings decreased the rate of Cr vaporization by more than one order of magnitude at 750 °C. No obvious difference in vaporization rate could be seen between the two coated materials, and no clear change in vaporization rate with time over 500–3300 h of exposure could be observed. To determine the activation energy for Cr vaporization from the Co- and the Ce/Co-coated material, Cr vaporization was also measured at 850 °C, but only for one week, in contrast to the samples exposed at 650 and 750 °C, which were exposed for 500 h. Fig. 3 shows an Arrhenius plot in which the natural logarithm of the Cr vaporization rate from the two coated materials (Co and Ce/Co) isothermally exposed at 850, 750, and 650 °C is plotted as a function of the inverse temperature. From the slope shown in this figure the activation energy (E_a) values for Cr vaporization from the Co- and Ce/Co-coated materials can be calculated using Equation (1).

$$\ln(k) = \frac{-E_a}{RT} + \ln(A) \quad (1)$$

where k is the Cr vaporization rate, E_a is the activation energy, R is the universal gas constant, T is the absolute temperature, and A is the pre-exponential factor. It can be seen that the two coated materials exhibit Arrhenius-type behaviour and the calculated activation energy value for the Co- and the Ce/Co-coated material was ~100 kJ/mol (92 kJ/mol for Co and 107 kJ/mol for Ce/Co).

3.3. Microstructural investigation

In Fig. 4, two STEM images of the oxide scale from the Co-coated material exposed for 3300 h at 650 °C are shown, as well as the corresponding EDX line scans showing the cation concentration of Co, Fe, Mn, and Cr. The two STEM images are taken from different areas of the oxide scale of the same sample, illustrating the rather large variations in thickness of the oxide scale observed for the exclusively Co-coated samples at 650 °C (see Fig. 5). From the results in Fig. 4 it can be seen that the oxide scale can be divided into at least three oxide layers.

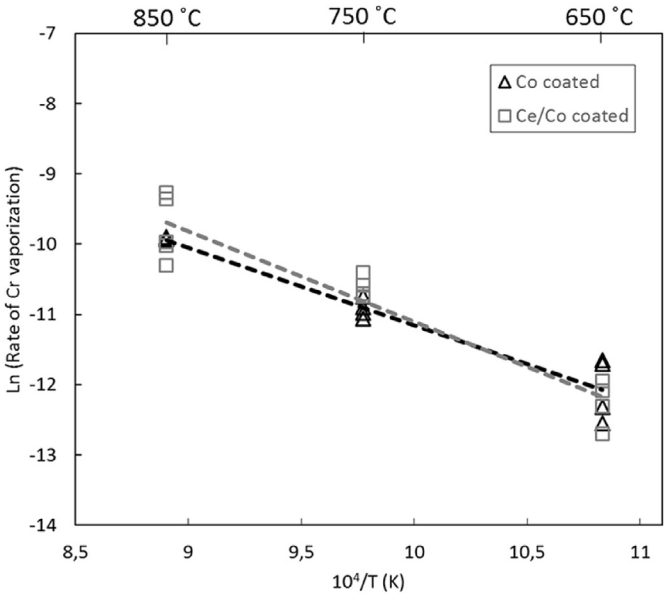

Fig. 3. Arrhenius plot showing the natural logarithm of the Cr vaporization rate as a function of the inverse temperature for Co-coated (black triangles) and Ce/Co-coated (grey squares) Sanergy HT isothermally exposed. The samples were exposed in air containing 3%H_2O and a flow rate of 6000 sml/min.

The outermost oxide layer consists of almost pure Co_3O_4 (spinel-phase confirmed with XRD) containing a few cation percent Fe and Mn, but no Cr was detected. Below this layer, both line scans (Fig. 4a and b) show a second Co oxide layer very rich in Fe. In the upper image (a), where this Fe-rich $(Co,Fe)_3O_4$ layer is rather thick, it can be seen that the Fe concentration is as high as 50%. It can also be seen that this layer is somewhat richer in Mn than the outermost Co_3O_4 layer. Below the $(Co,Fe)_3O_4$ layer, a third Co spinel layer can be seen (shown in 4b). This layer is rich in Co and Cr, as well as some Fe and Mn. Such a $(Co,Cr,Mn)_3O_4$ layer between the Co spinel layer and the Cr_2O_3 layer has been seen by other authors at higher temperatures [24,40–42]. According to the two line profiles shown in Fig. 4, the thin Cr_2O_3 layer seems to be very pure, consisting of almost 100 cation% Cr. Below this pure Cr_2O_3 layer, the Cr-rich oxide is enriched in Mn. In Fig. 4b a clear peak in Mn can be observed at the metal-oxide interface, which most probably is a thin layer of

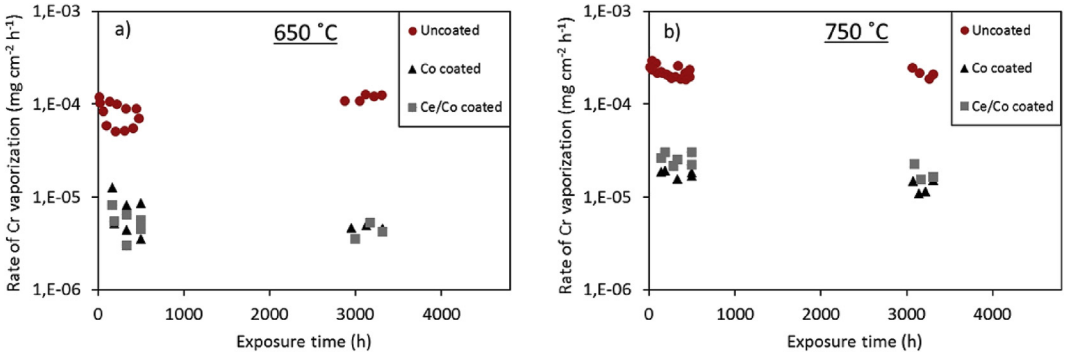

Fig. 2. Cr vaporization rate at (a) 650 °C and (b) 750 °C for uncoated (red dots), Co-coated (black triangles), and Ce/Co-coated (grey squares) Sanergy HT exposed for up to 3300 h in air containing 3% H_2O with a flow rate of 6000 sml/min. The first 500 h correspond to the isothermal exposures and the values between 2700 and 3300 h correspond to the measurements of the discontinuously exposed samples, after having been exposed for more than 2700 h. The isothermal exposure for the uncoated material is taken from a previous publication [37].

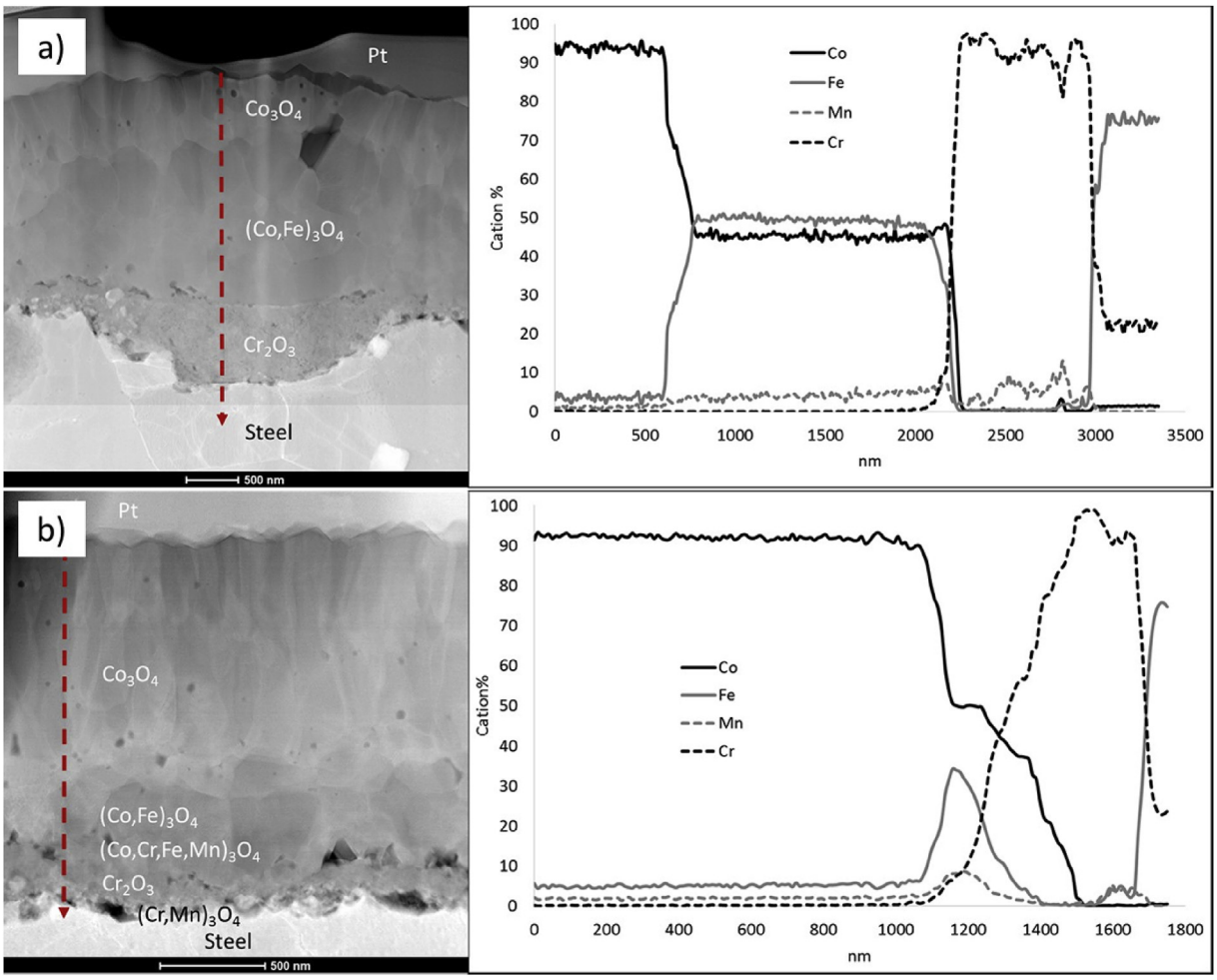

Fig. 4. STEM/EDX line scans along the oxide layer of Co-coated Sanergy HT exposed for 3300 h at 650 °C in air containing 3% H_2O with a flow rate set to 6000 sml/min. The two STEM images are taken from different areas of the oxide scale of the same sample, since rather large variations in thickness of the oxide scale were observed for the exclusively Co-coated samples exposed at 650 °C (See Fig. 5).

$(Cr,Mn)_3O_4$. Since these two layers (Cr_2O_3 and $(Cr,Mn)_3O_4$) are extremely thin at 650 °C, these two layers together will hereinafter be described as the Cr-rich oxide layer. In Fig. 5 Broad Ion Beam (BIB) cross sections and their corresponding EDX maps are shown for the Co- and the Ce/Co-coated material exposed for 500 and 3300 h at 650 °C.

Comparing the EDX maps in Fig. 5 with the EDX line scans in Fig. 4 for the Co-coated material exposed for 3300 h at 650 °C, it can be seen that the same four layers (a Co_3O_4 top layer, a Fe-rich $(Co,Fe)_3O_4$ layer below, a thin Cr_2O_3 layer, and a Cr and Mn rich oxide at the metal-oxide interface) are visible. No clear difference between the 500 and 3300 h exposure at 650 °C (Fig. 5) can be seen in the figures, which is in good agreement with the extremely small change in mass between 500 and 3300 h that is shown in Fig. 1. Furthermore, in the corresponding EDX maps the separation between a Co_3O_4 layer and a Fe-rich $(Co,Fe)_3O_4$ layer observed for the Co-coated material cannot be observed on the Ce/Co-coated material. Instead, the metallic Co-coating has been transformed to an almost pure Co_3O_4 oxide, similar to the outermost Co spinel layer, for the material coated only with Co. Due to the lack of the Fe-rich $(Co,Fe)_3O_4$ layer found for the Ce/Co-coated material, the Co oxide layer is thinner for the Ce/Co-coated material than for the Co-coated material, which agrees well with the lower initial mass gains for the Ce/Co-coated material (Fig. 1). In addition to the lack of a Fe-rich $(Co,Fe)_3O_4$ layer for the Ce/Co-coated material, the Cr-rich oxide layer is even thinner and more homogenous for the Ce/Co-coated than for the Co-coated material at 650 °C (Figs. 5 and 8). In fact, the thickness of the Cr-rich layer for the Co-coated material is between 100 and 700 nm, whereas for the Ce/Co-coated material the Cr-rich layer is approximately 100 nm without any large variations being observed. From the EDX maps (Fig. 5) it can be seen, as is the case for the exclusively Co-coated material, that most of the Mn accumulates at the metal-oxide interface, and very little Mn is to be found within the Co spinel. The concentration of Ce in the oxide scales formed on the Ce/Co-coated material is too low to be successfully mapped by SEM/EDX. Nevertheless, at the Co spinel – Cr_2O_3 interface, a faint bright layer was observed in the SEM using the backscattered mode (see Fig. 8). This bright layer, which was observed after 500 and 3300 h at 650 °C, is believed to be Ce oxide. The fact that this layer is visible in the SEM BSE images but cannot be mapped is due to the low concentration of Ce, as well as to the inherently inferior resolution of SEM/EDX analysis compared to SEM imaging.

The EDX maps of the Co- and Ce/Co-coated materials exposed for 500 and 3300 h at 750 °C can be seen in Fig. 6.

After 500 h at 750 °C the microstructure of the oxide scale is similar to the case at 650 °C. The Co oxide, for the material coated only with Co can be divided into two layers, one almost pure in Co

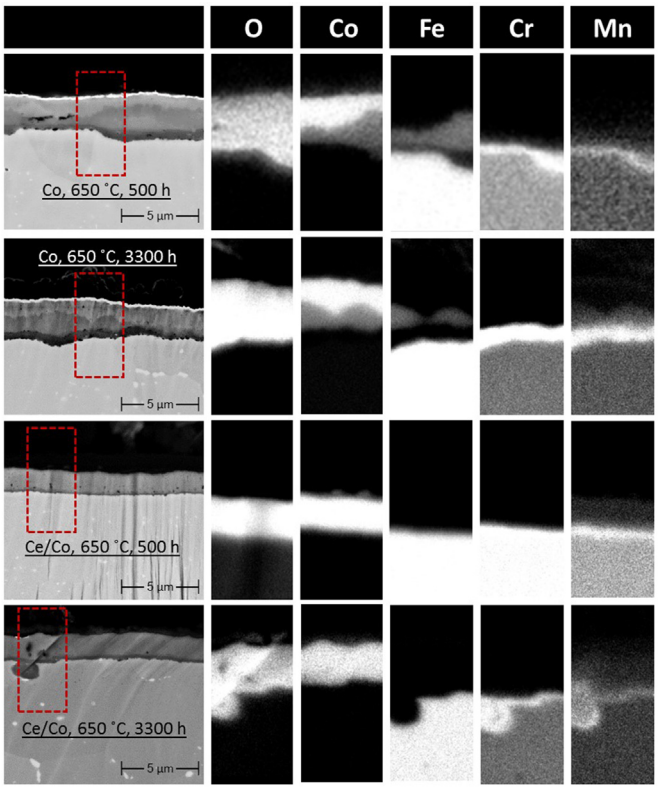

Fig. 5. Broad Ion Beam (BIB) cross-sections and their corresponding EDX maps for Co- and Ce/Co-coated Sanergy HT exposed for 500 and 3300 h at 650 °C in air containing 3% H_2O using a flow rate of 6000 sml/min. The Ce content was too low and the resolution of SEM/EDX analysis is inferior to the size of the Ce-rich particles/layer. Thus mapping Ce was not possible.

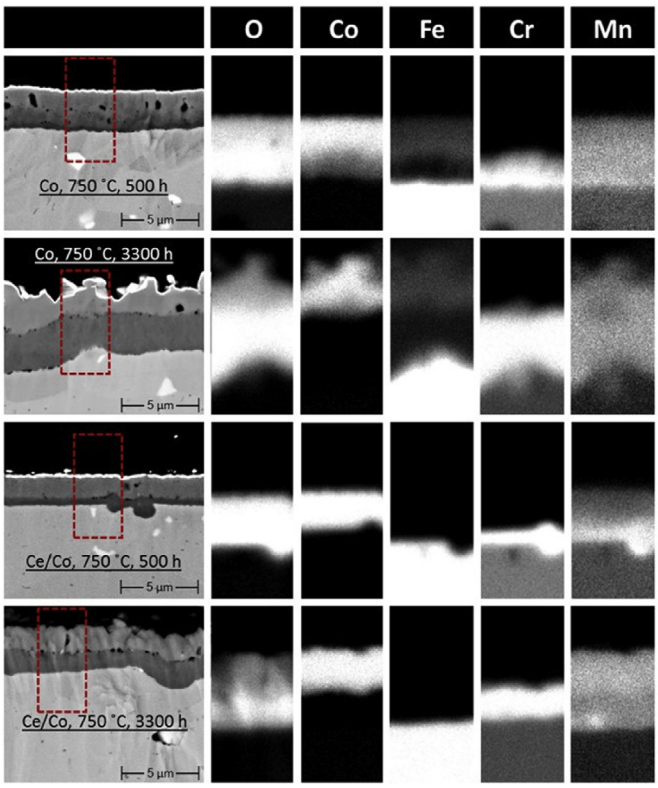

Fig. 6. Broad Ion Beam (BIB) cross-sections and their corresponding EDX maps of Co- and Ce/Co-coated Sanergy HT exposed for 500 and 3300 h at 750 °C in air containing 3% H_2O using a flow rate of 6000 sml/min. The Ce content was too low and the resolution of SEM/EDX analysis is inferior to the size of the Ce-rich particles/layer. Thus mapping Ce was not possible.

and one rich in both Fe and Co. In contrast to the exposure at 650 °C, however, there is no clear boundary between these two layers at 750 °C. Another difference to the 650 °C samples is that Mn is not only found mainly at the metal-oxide interface, it is also detected in the outermost Co spinel. After 3300 h at 750 °C, neither a Fe-rich Co spinel layer nor any enrichment of Mn at the metal-oxide interface could be observed. Instead both Fe and Mn were homogenously distributed within the Co spinel layer. The thickness of the Co spinel layer remained more or less unchanged over time, at approximately 2 µm. The roughness of the $(Co,Mn,Fe)_3O_4$ layer, however, significantly increased for the Co-coated material with time at 750 °C. Such an increase in surface roughness was not found on the Ce/Co-coated material after 3300 h at 750 °C. The increase in mass gain with time (after the rapid initial gain in mass due to Co oxidation), seen in Fig. 1, is attributed to an increase in the thickness of the Cr_2O_3 at 750 °C. This layer was, on average, thinner than 1 µm after 500 h for the Co-coated material but had grown to a thickness of 2–3 µm after 3300 h at 750 °C (Fig. 6). The most significant and important difference between the Ce/Co- and Co-coated material at 750 °C was the clear decrease in the Cr_2O_3 scale growth rate with the additional Ce layer. After only 500 h of exposure it could be seen that the Ce/Co-coated material displayed a thinner Cr_2O_3 scale (only 0.5 µm compared to 0.5–1 µm) and after 3300 h the Cr_2O_3 scale was almost 1 µm thinner for the Ce/Co-coated material than for the Co-material (1.5 µm compared to 2–3 µm). Using BSE imaging mode, which gives Z-contrast, a faint discontinuous bright layer and small bright particles were observed at the Cr_2O_3 - Co spinel interface of the Ce/Co-coated sample after 500 h at 750 °C (see Fig. 8). After 3300 h, however, only the bright particles were observed. Furthermore, these particles were observed not only at the Co spinel-Cr_2O_3 scale interface, but also within the Co spinel after 3300 h. These features are assumed to be Ce oxide particles, which agrees well with earlier TEM studies [21,43].

3.4. Area Specific Resistance (ASR) measurements

Fig. 7 shows the ASR measurements for both Co- and Ce/Co-coated material after 500 h of exposure at 650, 750, and 850 °C, measured at the corresponding exposure temperature (Fig. 7a) and measured at 650 °C (Fig. 7b).

From Fig. 7a it can be seen that all samples show low ASR values (below 20 mΩ cm^2) when measured at their corresponding exposure temperature. In Fig. 8, BIB cross-sections of the Co- and Ce/Co-coated materials exposed at 650, 750, and 850 °C for 500 h are shown. It can be seen that after 500 h at 850 °C the Cr_2O_3 layer is 3–4 µm for the Co-coated material and 2–3 µm for the Ce/Co-coated material compared to only a hundred to a few hundred nanometres for these materials exposed at 650 °C. When these samples were measured at 650 °C (Fig. 7b), instead of at the corresponding exposure temperature (850 °C), a significant increase in ASR due to the much thicker Cr_2O_3 scale on the samples could be seen. Furthermore, what seems to be a small difference in ASR between the Co- and the Ce/Co-coated material when measured at 850 °C is actually a significant difference when measured at 650 °C.

4. Discussion

The main reason for a Co-coating is to mitigate Cr vaporization. Earlier studies at 850 °C have clearly shown that thin metallic Co-

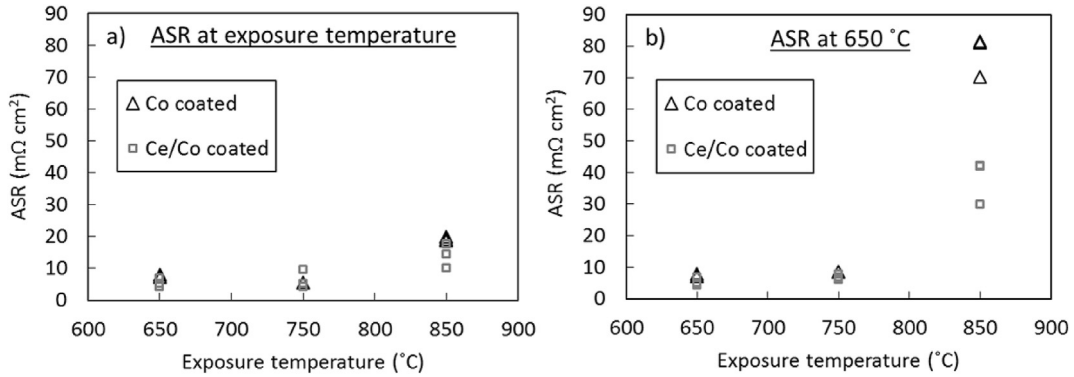

Fig. 7. ASR measurements carried out on Co-coated (black triangles) and Ce/Co-coated (grey squares) Sanergy HT exposed isothermally for 500 h in air containing 3% H_2O before Pt electrodes were contacted and ASR was measured. In (a) ASR was measured at the corresponding exposure temperature (650, 750 or 850 °C), and in (b), the ASR was measured at 650 °C for the very same samples as in (a).

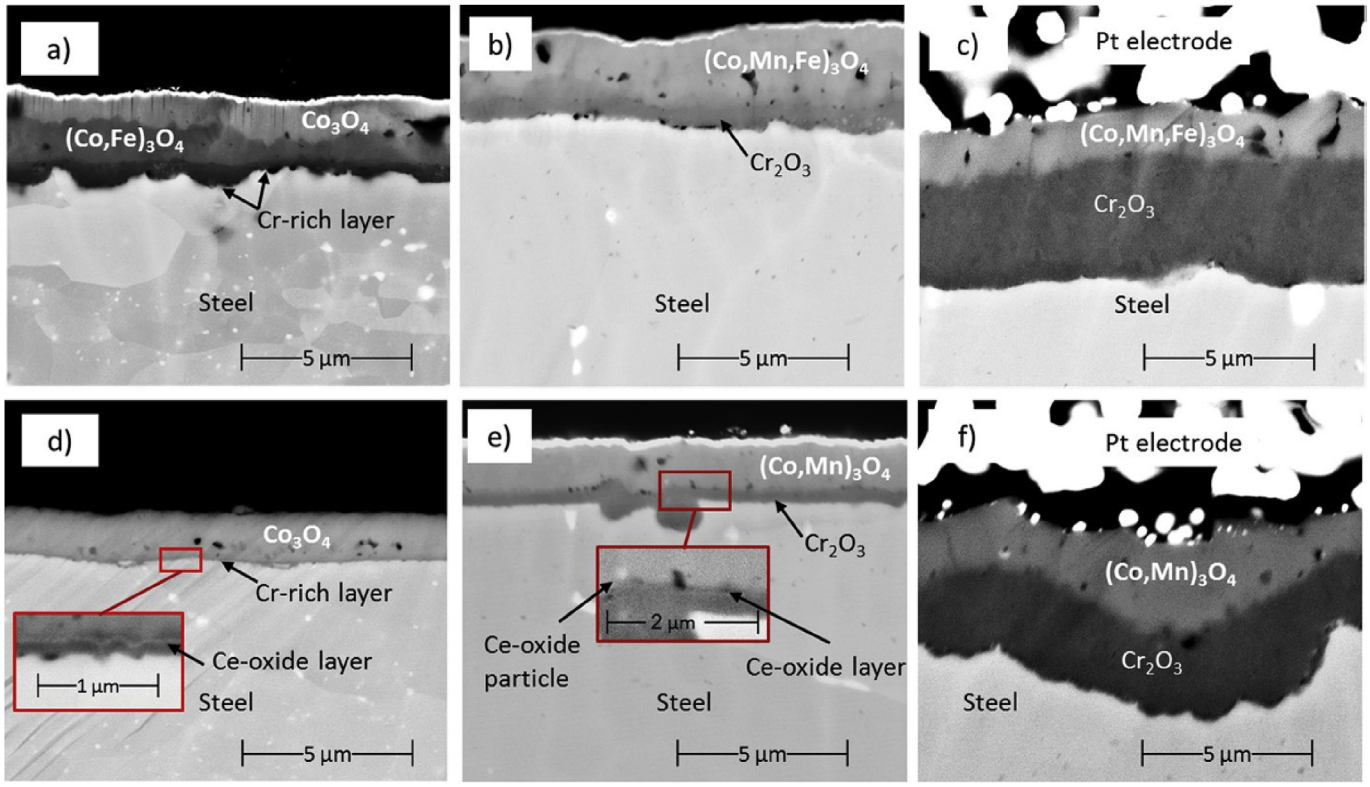

Fig. 8. Broad Ion Beam (BIB) cross-sections showing the oxide scales of the materials used for ASR measurements in Fig. 7. Images a-c show the oxide scales for the Co-coated material after 500 h at 650, 750, and 850 °C, and d-f show the oxide scales for the Ce/Co-coated material after 500 h at 650, 750, and 850 °C.

and Ce/Co-coatings are able to significantly lower the rate of Cr vaporization [20,21,23,25,26]. Initially the microstructure and chemical composition of the top Co spinel is more or less identical at 650–850 °C. However, at higher temperatures (750 and 850 °C), a change in the chemical composition of the top Co spinel layer was observed with time. This will be discussed in more detail below but, with the Cr vaporization measurements, it was proven that metallic Co-coatings significantly reduce Cr vaporization, regardless of whether the top layer is Co_3O_4, $(Co,Mn)_3O_4$, or $(Co,Mn,Fe)_3O_4$. The Cr vaporization rate at 750 and 650 °C was more than one magnitude lower for the Co- and Ce/Co-coated materials than the uncoated ones, even after 3300 h of exposure (Fig. 2). The Arrhenius plot in Fig. 3 also shows that Cr vaporization from Co- and Ce/Co-coated Sanergy HT followed Arrhenius behaviour. Activation energies of 92 and 107 kJ/mol for Cr vaporization from Co- and Ce/Co-coated Sanergy HT were calculated. These values can be compared to the 91 kJ/mol that was the calculated activation energy value for the uncoated Sanergy HT material in an earlier study [37]. All three values (uncoated, Co-coated, and Ce/Co-coated) are very close to the 83 kJ/mol theoretically calculated by Panas et al. [44], suggesting that the Cr vaporization mechanism is the same whether Cr is volatilized from Cr_2O_3, uncoated Sanergy HT or Co-coated Sanergy HT.

As briefly mentioned above, significant changes in both oxide

scale microstructure and chemical composition were found for the metallic Co- and Ce/Co-coated interconnects as a consequence of lowering the temperature. One important factor, which is largely influenced by temperature, is the outward diffusion of Mn into the oxidized Co-coating. At 650 °C only 2–3 cation % Mn was detected in the Co spinel after 3300 h (Fig. 4) for the Co-coated material. Instead of diffusing into the Co spinel layer, Mn was found as a Cr- and Mn-rich oxide at the metal-oxide interface. This Cr and Mn oxide is assumed to be $(Cr,Mn)_3O_4$, which should be the stable phase, according to Jung [45]. When the temperature was increased by 100 °C to 750 °C, such a Cr- and Mn-rich oxide layer was initially observed (after 500 h), however this layer disappeared after longer exposure times (3300 h), and a clear enrichment of Mn in the Co spinel was observed (Fig. 6). This can be compared to two TEM studies conducted at 850 °C on Sanergy HT coated with 640 nm Co [21,23]. In these two studies the Mn concentration in the Co spinel increased from around 15 to 26 cation % between 168 and 3000 h.

Another important effect of a decrease in temperature is the Fe concentration in the Co oxide. When a metallic Co-coating is exposed to elevated temperatures in air, the Co is rapidly oxidized. The conversion from metallic Co to a Co oxide for a 640 nm thick Co-coating takes less than 1 min at 850 °C [23]. During this short period of time Fe is able to diffuse into the Co-coating. However, once the Co is entirely oxidized and a continuous Cr_2O_3 layer has been established underneath, no more Fe is incorporated into the Co oxide. The result of this Fe outward diffusion is the formation of a dual-layered Co oxide consisting of an almost pure Co_3O_4 top layer and a Fe-rich $(Co,Fe)_3O_4$ layer underneath. This microstructure, which at 850 °C is observed after 1 h [23] and at 750 °C after 500 h (compare Fig. 6), is similar to the microstructure observed after 3300 h at 650 °C in this work (Fig. 5). With continued exposure time at higher temperatures (168 h at 850 °C [23] and 3300 h at 750 °C), Fe will be homogenously distributed throughout the Co spinel [24]. If the temperature is as low as 650 °C, however, this dual-layered structure of the Co oxide will be maintained for at least 3300 h. It is commonly claimed that the Cr_2O_3 layer is the main contributor to the electrical resistance of the oxide scale. While this is probably true for temperatures at 800 °C and above, where the Cr_2O_3 layer may be equally thick or even thicker than the coating, it may not necessarily be true at lower temperatures. At 650 °C the thickness of the two Co spinel layers after 500 as well as after 3300 h at 650 °C is around 2 μm, whereas the Cr-rich layer is only a hundred to a few hundred nm thick. It can therefore be speculated that the contribution of the Co spinel layer(s) to the total electrical scale resistivity may be much greater at 650 °C than at higher temperatures. Furthermore, as discussed above, very little Mn was found in the Co oxide at 650 °C, irrespective of whether the steel was coated only with Co or with Ce/Co. Petric and Ling [46] have studied the electrical conductivity of some spinel-type oxides at 800 °C in air. They found that the electrical conductivity for pure Co_3O_4 (6.7 S/cm) is one magnitude lower than $MnCo_2O_4$ (60 S/cm). At 650 °C no appreciable amounts of Mn diffused into the Co oxide. Instead, a Mn and Cr-rich layer was observed at the metal-oxide interface, most probably forming the even less conductive spinel oxide $(Cr,Mn)_3O_4$ (0.02 S/cm [46]). This was observed for both the Co- and Ce/Co-coated material. Consequently, it can be concluded that Mn diffusion is unaffected by the presence of the additional Ce-coating. However, when the additional layer of Ce was added to the Co-coating, the formation of a Fe-rich Co spinel layer was impeded, and the Co oxide was somewhat thinner as a consequence. This effect may lower the electrical resistance for the Ce/Co-coated material compared to the materials coated only with Co, since the electrical conductivity of the Fe-rich Co spinel, $CoFe_2O_4$, is even lower (0.93 S/cm) than pure Co_3O_4 (6.7 S/cm), according to the study by Petric and Ling [46]. The data published by Petric and Ling were collected from ceramic pellets and the measurements were carried out in air, and for this reason no variation in oxygen partial pressure within the samples can be assumed. This is not true for thermally grown oxide scales, where the oxygen partial pressure decreases from the surface of the sample to the metal bulk. Therefore, the values published by Petic and Ling should only be used as estimates. Although a significant reduction in electrical conductivity of the spinel layer as an effect of the change in chemical composition can be assumed, it should be noted that the electrical conductivity for Cr_2O_3 is significantly lower. The electrical conductivity for Cr_2O_3 at 800 °C is in the range 0.001–0.05 S/cm [47–50]. Assuming an electrical conductivity of 0.05 S/cm for the Cr_2O_3 scale, then the $CoFe_2O_4$ (0.93S/cm) layer needs to be almost 20 times thicker than the Cr_2O_3 scale, if electrical resistance should be associated to the Co spinel layer and not the Cr_2O_3 scale. For the even more conductive Co_3O_4 (6.7 S/cm) layer, which is formed on the Ce/Co coated material, the Co spinel layer needs be more than 100 times thicker than the Cr_2O_3 layer to dominate the total resistance. In fact, the ASR measurements of the samples exposed for 500 h at 650 °C showed that the lack of Mn in the Co spinel, as well as the formation of a Fe-rich $(Co,Fe)_3O_4$ layer on the Co-coated material, did not lead to notably higher electrical resistances. The electrical resistance for both the Co- and the Ce/Co coated material exposed for 500 h at 650 °C was only 4–8 mΩ cm^2, which can be considered to be very low. Nevertheless, it should be taken into consideration that the coatings in the present study were very thin, only 640 nm metallic Co, and in a case in which the metallic Co-coating would be in the μm-range, a greater effect of the Co spinel layers may be observed, especially considering the effect lower temperature has on the chemical composition of the Co spinel. However, from these results it can be concluded that as long as the metallic Co coating is thin, a low Mn and high Fe content in the Co spinel layer(s) is not an issue. Instead it seems that even at 650 °C a growing Cr_2O_3 scale is the main contributor to an increase in the electrical resistance. ASR measurements on uncoated Sanergy HT have previously been carried out by other researchers [34,51]. Skilbred et al. [51] measured an ASR of 6 mΩ cm^2 at 700 °C for uncoated Sanergy HT. This value is very close to the values in the present work for the Co- and the Ce/Co-coated materials exposed at 650 and 750 °C (See Fig. 7). This would support the assumption that the Co spinel does not contribute to the ASR to any measurable extent, and instead, the Cr_2O_3 scale is the dominating factor for the ASR, even at as low temperatures as 650 °C.

The greatest benefit of decreasing the SOFC operating temperature is probably the much slower oxide scale growth [37,51–53]. This was clearly seen when comparing the materials exposed at 650 °C and 750 °C. At 650 °C a very thin (100–700 nm) Cr-rich layer had formed within the first 500 h, consisting of both Cr_2O_3 and, most probably, $(Cr,Mn)_3O_4$. From both the mass gain values as well as the SEM cross-sections (Figs. 1 and 5), it can be concluded that this Cr-rich layer does not grow significantly with continued exposure time at 650 °C. Although the average Cr-rich oxide thickness was even thinner for the Ce/Co-coated material, both materials had developed very thin Cr-rich scales. It can therefore be questioned if an additional Ce layer is necessary when a SOFC operates at such low temperatures as 650 °C. However, within a SOFC stack, a temperature gradient of 50–100 °C is commonly observed. An increase in temperature by 50–100 °C from 650 °C would clearly lead to faster Cr_2O_3 scale growth, as seen in Figs. 1, 5, 6 and 8. This study shows that the additional 10 nm thin Ce-coating contributed to a significantly slower oxide scale growth rate at 750 °C. For the Co-coated material, the Cr_2O_3 layer grew by almost 2 μm between 500 and 3300 h at 750 °C. In contrast for the Ce/Co coated material, the Cr_2O_3 layer only grew by 1 μm during this time. Additions of reactive elements such as Ce, La, Y, Hf, and Zr, are

known to significantly improve oxidation resistance at high temperatures. Several mechanisms have been proposed in attempts to explain the reactive element effect [35,54–56]. The most widespread theory suggests that undoped Cr_2O_3 grows by a combination of metal cation and oxygen diffusion, with the former being the dominant mechanism. Doping with reactive elements causes a segregation of the reactive elements at the Cr_2O_3 grain boundaries. This impedes metal cation outward diffusion and, as a consequence, the smaller flux of oxygen ions becomes dominant. This not only reduces oxide scale growth but also results in better scale adhesion. The latter effect is attributed to the fact that the impeded Cr outward flux corresponds to a reduced inward flux of metal vacancies. This in turn reduces the amount of voids at the metal/oxide interface which in the absence of reactive elements are expected to form due to vacancy condensation. Whether this theory can be applied for the Ce/Co-coatings investigated here is presently unknown. Sattari et al. [43] studied 10 nm Ce-coated Sanergy HT that was exposed at 850 °C. In that study Ce was found, using TEM/EELS, both as Ce oxide particles at the surface of the oxide scale, and segregated at the grain boundaries of the $(Cr,Mn)_3O_4$ top-layer in the vicinity of the scale gas interface. Despite the dedicated analysis, no Ce was detected within the Cr_2O_3 scale, which is hard to reconcile with the above cited theory. Further studies are therefore needed to fully understand the mechanism of how the Ce/Co-coating affects oxidation.

As shown above, the Cr_2O_3 layer is expected to dominate the ASR of the oxide scale. Thus it is conceived that reactive element additions, which result in a thinner Cr_2O_3 scale, have a beneficial effect on ASR. Earlier studies of Co- and Ce/Co-coated Sanergy HT at 850 °C have shown that the addition of 10 nm Ce lowers electrical resistance significantly [33,34], and for that reason the same beneficial effect on electrical resistance is expected at 750 °C. In the present study ASR measurements were carried out after 500 h of exposure. Both Co- and Ce/Co-coated samples showed rather thin Cr_2O_3 scales (<1 μm) after 500 h at 750 °C, and consequently no clear difference in ASR was measured. However, the ASR measurements of the Co- and Ce/Co-coated samples exposed for 500 h at 850 °C, which had developed μm-thick Cr_2O_3 scales, clearly showed the effect a thicker Cr_2O_3 scale has on electrical resistance. Therefore it can be assumed that the observed slower Cr_2O_3 scale growth rate for the Ce/Co-coated material at 750 °C, over the long term, will significantly reduce electrical scale resistance compared to the exclusively Co-coated material. As mentioned above Ce additions could improve interfacial contact by supressing the formation of voids at the metal-oxide interface which might result in lower ASR. After long-term exposure (Figs. 5 and 6) indeed slightly less pores have been observed at the metal-oxide interface on Ce/Co-coated samples.

The Cr_2O_3 scale thicknesses in this work for the Co- and Ce/Co-coated materials after 500 h at 750 °C (<1 μm) can be compared to the Cr_2O_3 scales observed by Skilbred et al. [51] on uncoated Sanergy HT after 500 h at 700 °C (extremely thin) and 800 °C (1.3 μm). Furthermore, the thickness of the Cr_2O_3 scale agrees very well with the ~200 nm thin Ce/Co dip-coated ferritic stainless steel 430 exposed for 1000 h at 750 °C in the study by Qu et al. [57]. In that study the Cr_2O_3 scale thickness after 1000 h was 1–1.5 μm. In the same study Qu et al. investigated Y/Co-coatings, which showed an even better oxidation resistance than the Ce/Co-coated material (<1 μm after 1000 h at 750 °C). In a second study by Qu et al. [58] the ferritic stainless steel 430 SS was dip-coated with Co, Y, and Y/Co. In contrast to the results presented in this work, the Cr_2O_3 scale had grown significantly thicker (2.25 μm) after 500 h at 750 °C for the exclusively Co-coated material, compared to the Y/Co-coated material (0.75 μm). In that study ASR was measured on both Co- and Y/Co-coated materials. However, these values were higher (71 and 16 mΩ cm^2 respectively for the exclusively Co-coated and the Y/Co-coated material after 250 h at 750 °C) than the ASR values presented in Fig. 7. The Cr_2O_3 scale thickness as well as the ASR values at 750 °C in the present work can also be compared to the results presented by Dayaghi et al. [28]. In that study the ferritic stainless steel AISI 430 was coated with a MnCo-coating using sol-gel deposition. After 750 h at 750 °C a thermally grown oxide scale of approximately 1 μm thickness had been formed, and the ASR (measured at 800 °C), was 4.9 mΩ cm^2. It is not trivial to compare ASR values, since in most cases different setups and methods are used. However, what can be concluded from the findings in this work and the above cited studies is that as long as the Cr_2O_3 scale is ~1 μm or thinner, low ASR values can be expected irrespective of the chemical composition, or coating method, of the Co-spinel or MCO-coating.

Furthermore, from the ASR measurements in Fig. 7b it is critical to point out how important it is to actually measure ASR at the desired stack operating temperature. When the ASR was measured at 850 °C no large difference was seen between the Co- and the Ce/Co-coated materials, with both showing ASR values between 10 and 20 mΩ cm^2. However, when measured at 650 °C the same samples showed ASR values between 30 and 80 mΩ cm^2, and a significant difference between the two coated materials was seen. It is therefore important to measure the ASR at the desired operating temperature, especially in the case when increased temperature is used to accelerate the test. In this work all samples isothermally exposed at 650 °C showed very low ASR values. The reason for this is the very thin Cr-rich oxide layer. In several studies coatings have been applied as powder, with the need for an extra heat treatment to densify the coating [59–61]. In those studies μm thick Cr_2O_3 layers were formed due to the heat treatment necessary to densify the powder. As the ASR measurements from Fig. 7 show, this would have a tremendous effect on electrical resistance at 650 °C. Therefore, metallic conversion coatings, as well as coatings deposited with other techniques that do not require a high temperature heat treatment, seem to be the most suitable coating techniques for IT-SOFC.

5. Conclusions

In this study uncoated, 640 nm Co-coated, and 10 nm + 640 nm Co-coated Sanergy HT were exposed up to 3300 h in air at 650 and 750 °C. Chromium species volatilization, oxide scale growth, and electrical scale resistance were studied. The following conclusions were drawn:

- A decrease in temperature not only leads to thinner oxide scales and less chromium species volatilization but also to a significant change in the microstructure and chemical composition of the oxide scale.
- During the initial oxidation phase the metallic Co-coating was converted into a Co_3O_4 top layer and a Fe-rich $(Co,Fe)_3O_4$ sub-layer. By adding a layer of 10 nm Ce, between the steel and the Co-coating, the diffusion of Fe was inhibited, and as a consequence only Co_3O_4 was formed.
- At 650 °C, once the initial oxidation phase was completed, no visible changes in oxide scale thickness or in the chemical composition of the oxide scales were observed for 3300 h. The thickness of the Cr_2O_3 scales after the initial oxidation phase, also after 3300 h, was only 100–700 nm.
- At 750 °C the Cr_2O_3 scale continued to grow with time, leading to scale thicknesses between 2 and 3 μm after 3300 h for the exclusively Co-coated material. The addition of a Ce-layer improved oxidation resistance significantly at 750 °C, reducing the Cr_2O_3 scale thickness to 1.5 μm after 3300 h.

- By coating the steel with Co or Ce/Co, the Cr vaporization rate was decreased by more than a factor of 10 compared to the uncoated material at 650 and 750 °C.
- Very low Area Specific Resistance (ASR) values (below 10 mΩ cm^2) were measured for both Co- and Ce/Co-coated steel at 650 and 750 °C after 500 h of exposure. This indicates that the variations in Co spinel composition described above do not have any noticeable influence on ASR. Instead it is suggested that the thin Cr_2O_3 scales are the main contributor to the ASR.
- If higher temperature is used to accelerate the corrosion test it is critical that the ASR is measured at the desired operating temperature. In this study ASR values in the 10–20 mΩ cm^2 range (measured at 850 °C) increased to 30–80 mΩ cm^2 when measured at 650 °C.
- To limit electrical scale resistance at 650 °C the Cr_2O_3 scale should not be thicker than 1 μm, and consequently coating techniques in which no additional heat treatment to densify the coating is necessary are suggested as suitable for interconnects intended for use in IT- SOFC.

Acknowledgements

AB Sandvik Materials Technology is acknowledged for providing the materials. The research leading to these results has received funding from the Swedish Research Council and the Swedish Energy Agency. Emelie Smedberg Björn and Bridget Dwamena are gratefully acknowledged for their contribution to this work within their bachelor theses.

References

[1] M. Powell, K. Meinhardt, V. Sprenkle, L. Chick, G. McVay, J. Power Sources 205 (2012) 377–384.
[2] A.B. Stambouli, E. Traversa, Renew. Sust. Energ Rev. 6 (2002) 433–455.
[3] J.W. Fergus, Mat. Sci. Eng. A Struct. 397 (2005) 271–283.
[4] B.B. Ebbinghaus, Combust. Flame 93 (1993) 119–137.
[5] C. Gindorf, L. Singheiser, K. Hilpert, J. Phys. Chem. Solids 66 (2005) 384–387.
[6] K. Hilpert, D. Das, M. Miller, D.H. Peck, R. Weiss, J. Electrochem Soc. 143 (1996) 3642–3647.
[7] E.J. Opila, D.L. Myers, N.S. Jacobson, I.M.B. Nielsen, D.F. Johnson, J.K. Olminsky, M.D. Allendorf, J. Phys. Chem. A 111 (2007) 1971–1980.
[8] S.P.S. Badwal, R. Deller, K. Foger, Y. Ramprakash, J.P. Zhang, Solid State Ion. 99 (1997) 297–310.
[9] X.B. Chen, L. Zhang, E.J. Liu, S.P. Jiang, Int. J. Hydrogen Energ 36 (2011) 805–821.
[10] J.W. Fergus, Int. J. Hydrogen Energ 32 (2007) 3664–3671.
[11] M. Krumpelt, T.A. Cruse, B.J. Ingram, J.L. Routbort, S.L. Wang, P.A. Salvador, G. Chen, J. Electrochem Soc. 157 (2010) B228–B233.
[12] A.A. Kulikovsky, J. Electrochem Soc. 158 (2011) B253–B258.
[13] J.A. Schuler, C. Gehrig, Z. Wuillemin, A.J. Schuler, J. Wochele, C. Ludwig, A. Hessler-Wyser, J. Van Herle, J. Power Sources 196 (2011) 7225–7231.
[14] S.P. Simner, M.D. Anderson, G.G. Xia, Z. Yang, L.R. Pederson, J.W. Stevenson, J. Electrochem Soc. 152 (2005) A740–A745.
[15] M.C. Tucker, H. Kurokawa, C.P. Jacobson, L.C. De Jonghe, S.J. Visco, J. Power Sources 160 (2006) 130–138.
[16] H. Kurokawa, C.P. Jacobson, L.C. DeJonghe, S.J. Visco, Solid State Ion. 178 (2007) 287–296.
[17] R. Trebbels, T. Markus, L. Singheiser, J. Electrochem Soc. 157 (2010) B490–B495.
[18] J. Puranen, M. Pihlatie, J. Lagerbom, T. Salminen, J. Laakso, L. Hyvarinen, M. Kylmalahti, O. Himanen, J. Kiviaho, P. Vuoristo, Int. J. Hydrogen Energ 39 (2014) 17246–17257.
[19] P.E. Gannon, V.I. Gorokhovsky, M.C. Deibert, R.J. Smith, A. Kayani, P.T. White, S. Sofie, Z. Yang, D. McCready, S. Visco, C. Jacobson, H. Kurokawa, Int. J. Hydrogen Energ 32 (2007) 3672–3681.
[20] M. Stanislowski, J. Froitzheim, L. Niewolak, W.J. Quadakkers, K. Hilpert, T. Markus, L. Singheiser, J. Power Sources 164 (2007) 578–589.
[21] S. Canovic, J. Froitzheim, R. Sachitanand, M. Nikumaa, M. Halvarsson, L.G. Johansson, J.E. Svensson, Surf. Coat. Technol. 215 (2013) 62–74.
[22] J.W. Wu, C.D. Johnson, R.S. Gemmen, X.B. Liu, J. Power Sources 189 (2009) 1106–1113.
[23] J. Froitzheim, S. Canovic, M. Nikumaa, R. Sachitanand, L.G. Johansson, J.E. Svensson, J. Power Sources 220 (2012) 217–227.
[24] A. Harthøj, T. Holt, P. Møller, J. Power Sources 281 (2015) 227–237.
[25] H. Falk-Windisch, M. Sattari, J.E. Svensson, J. Froitzheim, J. Power Sources 297 (2015) 217–223.
[26] J.G. Grolig, J. Froitzheim, J.E. Svensson, J. Power Sources 248 (2014) 1007–1013.
[27] A. Kruk, A. Adamczyk, A. Gil, S. Kac, J. Dabek, M. Ziabka, T. Brylewski, Thin Solid Films 590 (2015) 184–192.
[28] A.M. Dayaghi, M. Askari, H. Rashtchi, P. Gannon, Surf. Coat. Tech. 223 (2013) 110–114.
[29] S.M. Technology, in http://smt.sandvik.com/en/products/strip-steel/strip-products/coated-strip-steel/production-process/.
[30] H. Falk-Windisch, I. Mertzidis, J.E. Svensson, J. Froitzheim, Ecs Trans. (2015) 1617–1623.
[31] J. Froitzheim, J.E. Svensson, Ecs Trans. 35 (2011) 2503–2508.
[32] J.G. Grolig, J. Froitzheim, J.-E. Svensson, J. Power Sources 284 (2015) 321–327.
[33] J.G. Grolig, J. Froitzheim, J.E. Svensson, Electrochim. Acta 184 (2015) 301–307.
[34] A. Magrasó, H. Falk-Windisch, J. Froitzheim, J.-E. Svensson, R. Haugsrud, Int. J. Hydrogen Energ 40 (2015) 8579–8585.
[35] B. Pint, in: P.F. Tortorelli, P.Y. Hou (Eds.), Proceedings of the John Stringer Symposium, ASM, Materials Park, OH, Citeseer, 2003.
[36] J. Froitzheim, H. Ravash, E. Larsson, L.G. Johansson, J.E. Svensson, J. Electrochem Soc. 157 (2010) B1295–B1300.
[37] H. Falk-Windisch, J.E. Svensson, J. Froitzheim, J. Power Sources 287 (2015) 25–35.
[38] B. Pujilaksono, T. Jonsson, M. Halvarsson, I. Panas, J.E. Svensson, L.G. Johansson, Oxid. Met. 70 (2008) 163–188.
[39] C.S. Tedmon, J. Electrochem Soc. 113 (1966) 766.
[40] Y.Z. Hu, C.X. Li, G.J. Yang, C.J. Li, Int. J. Hydrogen Energ 39 (2014) 13844–13851.
[41] C. Macauley, P. Gannon, M. Deibert, P. White, Int. J. Hydrogen Energ 36 (2011) 4540–4548.
[42] K.L. Wang, Y.J. Liu, J.W. Fergus, J. Am. Ceram. Soc. 94 (2011) 4490–4495.
[43] M. Sattari, R. Sachitanand, J. Froitzheim, J.E. Svensson, T. Jonsson, Mater High. Temp. 32 (2015) 118–122.
[44] I. Panas, J.E. Svensson, H. Asteman, T.J.R. Johnson, L.G. Johansson, Chem. Phys. Lett. 383 (2004) 549–554.
[45] I.H. Jung, Solid State Ion. 177 (2006) 765–777.
[46] A. Petric, H. Ling, J. Am. Ceram. Soc. 90 (2007) 1515–1520.
[47] J.H. Park, K. Natesan, Oxid. Met. 33 (1990) 31–54.
[48] A. Holt, P. Kofstad, Solid State Ion. 69 (1994) 137–143.
[49] H. Nagai, T. Fujikawa, K. Shoji, T Jpn. I Met. 24 (1983) 581–588.
[50] P. Huczkowski, N. Christiansen, S.V.L. Niewolak, J. Piron-Abellan, L. Singheiser, W.J. Quadakkers, Fuel Cells 6 (2006) 93–99.
[51] A.W.B. Skilbred, R. Haugsrud, J. Power Sources 206 (2012) 70–76.
[52] P. Jian, L. Jian, H. Bing, G.Y. Xie, J. Power Sources 158 (2006) 354–360.
[53] T. Brylewski, M. Nanko, T. Maruyama, K. Przybylski, Solid State Ion. 143 (2001) 131–150.
[54] E.A. Polman, T. Fransen, P.J. Gellings, J. Phys Condens. Mat. 1 (1989) 4497–4510.
[55] R.W. Jackson, J.P. Leonard, L. Niewolak, W.J. Quadakkers, R. Murray, S. Romani, G.J. Tatlock, F.S. Pettit, G.H. Meier, Oxid. Met. 78 (2012) 197–210.
[56] C.M. Cotell, G.J. Yurek, R.J. Hussey, D.F. Mitchell, M.J. Graham, Oxid. Met. 34 (1990) 201–216.
[57] W. Qu, H. Li, D.G. Ivey, J. Power Sources 138 (2004) 162–173.
[58] W. Qu, L. Jian, D.G. Ivey, J.M. Hill, J. Power Sources 157 (2006) 335–350.
[59] Y. Zhang, A. Javed, M.M. Zhou, S.Q. Liang, P. Xiao, Int. J. Appl. Ceram. Tec. 11 (2014) 332–341.
[60] L. Chen, E.Y. Sun, J. Yamanis, N. Magdefrau, J. Electrochem Soc. 157 (2010) B931–B942.
[61] S.R. Akanda, N.J. Kidner, M.E. Walter, Surf. Coat. Tech. 253 (2014) 255–260.